Gypsum under pressure: A first-principles study

Luigi Giacomazzi and Sandro Scandolo
CNR-INFM/Democritos National Simulation Center, The Abdus Salam International Centre for Theoretical Physics (ICTP), Strada Costiera 11, I-34151 Trieste, Italy

(Received 18 November 2009; revised manuscript received 12 January 2010; published 3 February 2010)

We investigate by means of first-principles methods the structural response of gypsum ($CaSO_4 \cdot 2H_2O$) to pressures within and above the stability range of gypsum-I ($P \leq 4$ GPa). Structural and vibrational properties calculated for gypsum-I are in excellent agreement with experimental data. Compression within gypsum-I takes place predominantly through a reduction in the volume of the CaO_8 polyhedra and through a distortion of the hydrogen bonds. The distance between $CaSO_4$ layers becomes increasingly incompressible, indicating a mechanical limit to the packing of water molecules between the layers. We find that a structure with collapsed interlayer distances becomes more stable than gypsum-I above about 5 GPa. The collapse is concomitant with a rearrangement of the hydrogen-bond network of the water molecules. Comparison of the vibrational spectra calculated for this structure with experimental data taken above 5 GPa supports the validity of our model for the high-pressure phase of gypsum.

DOI: 10.1103/PhysRevB.81.064103 PACS number(s): 61.50.Ks, 62.50.−p, 64.70.K−

I. INTRODUCTION

Understanding the high-pressure (HP) behavior of hydrous minerals is important both for its planetary[1] and geophysical implications.[2,3] For instance, hydrous minerals are known to play an important role in the hydration and hence in the seismic anisotropy of subducting oceanic plates.[4] Moreover it was suggested that the earth's lower mantle could store more water than the oceans.[2] As a consequence, several experimental and theoretical investigations have addressed the response of hydrous minerals to earth's mantle pressures. Several phase transitions were discovered or are under debate, e.g., in $Al(OH)_3$ (gibbsite) at about 2.5 GPa,[5,6] in $Al_2Si_2O_5(OH)_4$ (dickite) at about 2.0 GPa.[7] Furthermore, a disordering of the hydrogen sublattice was observed in $Ca(OH)_2$ (portlandite) and $Co(OH)_2$ for pressures higher than about 10 GPa.[8–11] High-pressure proton disorder was also found in $Mg(OH)_2$ (brucite), a model system for hydrous phases of the earth's crust and mantle.[11–13] Phase transitions were also reported for $CaSO_4 \cdot 2H_2O$ (gypsum) at about 4 GPa,[14–16] and $CaAl_2Si_2O_7(OH)_2 \cdot H_2O$ (lawsonite) at 4 and 9.5 GPa.[17]

Hydrous minerals contain water either in the form of hydroxyl (-OH) groups, or in molecular form (H_2O).[18,19] While the effects of pressure on hydroxyl-containing minerals is widely studied,[5–13,20] less is known about the mechanisms through which molecular water is retained in some hydrous minerals at high pressure, with the exception of recent studies on lawsonite,[21] on the 10 Å phase,[22,23] and on gypsum.[19,24] At variance with lawsonite and the 10 Å phase, water in gypsum is incorporated exclusively in the molecular form.

Gypsum is among the most abundant minerals of ancient marine evaporite deposits.[25] Sedimentary beds or layers of gypsum are formed by direct precipitation out of evaporating seawater in lagoons where waters of high calcium and sulfate content can slowly evaporate and be continuously refilled with new sources of water. Sedimentary gypsum is nowadays mined for commercial purposes. Mineral gypsum has the remarkable property of forming crystals of extremely large size.[26] The crystalline structure of gypsum is composed of calcium sulfate ($CaSO_4$) layers linked together through hydrogen bonds by a layer of water molecules.[27–31] Calcium ions form CaO_8 polyhedra. Six oxygens of the CaO_8 polyhedron are shared with sulfate groups (SO_4) and the remaining two oxygens are shared with water molecules. The high-pressure behavior of gypsum was the subject of a neutron-diffraction study up to 5 GPa (Ref. 32). A more recent powder x-ray diffraction and Raman study[14] has revealed polymorphic pressure-induced transitions in the range 5–10 GPa. Discontinuities in the behavior of gypsum at high pressure have been confirmed by infrared (IR) and Raman spectroscopy.[15] A very recent investigation has provided additional evidence for a phase transition at about 4–5 GPa.[16] Several hypotheses have been put forward to explain the nature of the phase transition. A first interpretation invokes distortions of the sulfate tetrahedra and rearrangements of the sulfate and water molecules in the gypsum lattice.[14,16] According to an alternative explanation, high pressure would cause a displacement of the water molecules giving rise to a disordered water layer.[15]

First-principles theoretical investigations are nowadays routinely used in the field of high-pressure mineral physics[33,34] and have been applied successfully to understand the high-pressure behavior of several hydrous minerals. For instance, in brucite and portlandite, the pressure-induced hydrogen sublattice amorphization was shown to be caused by a frustration phenomenon.[12] Moreover, the structure and the physical properties of the 10 Å phase were recently investigated by *ab initio* simulation over a wide range of pressure and water content, bringing support to the idea that a variable amount of water can be incorporated into the 10 Å phase.[22]

The purpose of this paper is to investigate the pressure-induced changes in gyspum by means of first-principles simulations. The paper is divided in two parts. In the first part, we investigate the pressure behavior of the gypsum phase stable at ambient conditions, gypsum-I. Our results for the structural parameters and vibrational spectra of gypsum-I are in very good agreement with the experiments. In the

second part, we generate a theoretical model for the high-pressure phase of gypsum above 5 GPa. Comparison with experiments supports the hypothesis of a disordering of the water layers in gypsum at high pressure.

The paper is organized as follows. In Sec. II we report the technical details of our *ab initio* calculations. In Sec. III A we address the structural properties of gypsum-I under compression and report the pressure behavior of the unit-cell parameters, hydrogen-bond lengths and angles, sulfate volume and bond lengths, Ca polyhedra volumes, and interlayer thickness. Section III B focuses on the infrared and Raman spectra. We compute the high-frequency dielectric constant and its pressure derivative. We present the zone-center vibrational density of states, which is analyzed in terms of local contributions. We also present the pressure dependence of the frequencies of the Raman and infrared modes above 400 cm^{-1}. In Sec. IV, we investigate the high-pressure phase of gypsum by analyzing the structural and vibrational properties of a model generated by means of first-principles molecular dynamics (MD). Finally, Sec. V contains the conclusions of our work.

II. METHODS

We have performed first-principles electronic-structure calculations based on density-functional theory. We used the computational codes and pseudopotentials available in the QUANTUM-ESPRESSO package.[35,36] The exchange and correlation functional was approximated through the generalized gradient approximation.[37] Structural optimizations (lattice and internal parameters) were carried out by means of variable-cell relaxation. Vibrational modes were calculated by linear-response theory[38] and Raman spectra were evaluated in the nonresonant condition using second-order response theory.[39] Core-valence interactions were described by means of norm-conserving pseudopotentials. The electronic wave functions were expanded using a plane-wave basis set with energy cutoff of 100 Ry. The Brillouin zone was sampled by $3\times3\times3$ k-points grid. Calculations for gypsum-I were carried out with the primitive unit cell containing 24 atoms (see Sec. III A). The search for the high-pressure phase was performed by first-principles MD at constant pressure,[40,41] followed by structural relaxation with a simulation cell containing 48 atoms (see Sec. IV). For the MD simulations we employed ultrasoft pseudopotentials with a wave-function cutoff of 25 Ry and a charge density cutoff of 200 Ry.[42] The Brillouin zone of the supercell, containing 48 atoms, was sampled using the Γ point only. Structural relaxation of the structures obtained in the MD runs were then carried out with the approximations described above, i.e., with converged Brillouin-zone sampling and norm-conserving pseudopotentials.

III. GYPSUM-I UNDER PRESSURE

A. Structural properties

As a starting point for our analysis of the structural properties of gypsum-I (centered monoclinic lattice, space group $C2/c$), we considered the lattice and internal parameters determined at ambient conditions in Ref. 16. In Fig. 1 we show the primitive unit cell of gypsum-I containing two molecular units $CaSO_4\cdot2H_2O$. The sulfate layers are oriented parallel to the (010) crystallographic planes.

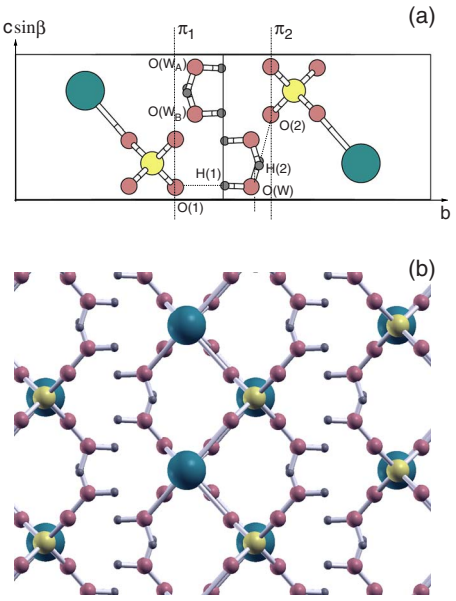

FIG. 1. (Color online) (a) Gypsum primitive unit cell. Hydrogen bonds O(w)-H(1)···O(1) and O(w)-H(2)···O(2) are shown. π_1 and π_2 are the oxygen planes defining the interlayer region and the polyhedral layer. (b) Extended view of the gypsum structure at ambient conditions. The size of the balls is in the order: Ca (largest), S, O, and H.

In Fig. 2 we show the cell parameters a, b, c, and β for gypsum-I as a function of pressure, as calculated in this study and as determined in a recent single-crystal x-ray study.[16] Theoretical and experimental data agree within less than 1%. We calculated the axial compressibilities by fitting the cell parameters a,b,c with equations of the form

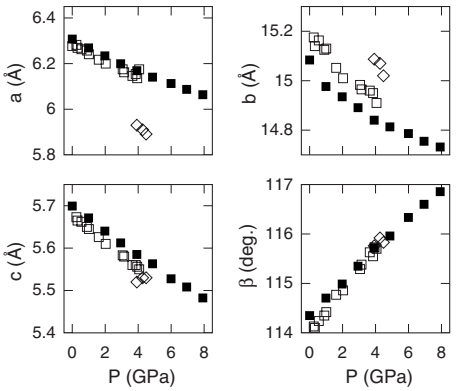

FIG. 2. Gypsum cell parameters a, b, c, and β vs applied pressure as calculated from first principles (filled squares) and as measured in experiment (open symbols, Ref. 16). Also reported the cell parameters (diamonds) above 4 GPa, that have been assigned to a new high-pressure phase (Ref. 16).

TABLE I. Compressibilities of the unit-cell parameters obtained by fitting the data up to 4 GPa and expressed in units of 10^{-3} GPa^{-1}. Experimental compressibilities from Ref. 16 are reported for comparison. Experimental error is indicated in parenthesis.

	β_{0a}	β_{0b} [a]	β_{0c}
	5.7	5.0	5.3
Expt.	6.1(1)	6.2(8)	5.6(1)

[a] β_{0b} is obtained by fitting data in the range 0–2 GPa.

$$\frac{1}{a} = \frac{1}{a_0}(\beta_{0a}P + 1) \quad (1)$$

and similarly for b and c (where P is the pressure and the subscript "0" indicates ambient pressure). The compressibilities β_0 found by best fit to the theoretical data are listed in Table I and compared with experimental results. The compressibilities along the a and c axes agree within about 5% with the experiments, while a larger difference is found for the compressibility along b, where, however, the experimental error is also larger. Theoretical and experimental data for β_{0b} were fitted considering data only up to 2 GPa because of nonlinearity above this pressure.[16] A fit of β_{0b} carried out considering data up to 8 GPa gives a value of 2.1 $\times 10^{-3}$ GPa^{-1}, about half the value determined with data up to 2 GPa, confirming the strongly nonlinear dependence of b with pressure. By contrast, fits of β_{0a} and β_{0c} up to 8 GPa show a reduction of only 20% and 10%, respectively.

At ambient conditions water molecules form weak hydrogen bonds with the O atoms of the Ca and S polyhedra (Fig. 1). The water molecules are all structurally equivalent but are distorted[43] from the geometry of a free water molecule with an H(1)-O(w)-H(2) bond angle of 106.6° and nonequivalent H(1)-O(w) and H(2)-O(w) bond lengths of 0.978 and 0.973 Å, respectively. This values compare well with experimental estimates for the bond angle (107.5°) and bond lengths (0.959 Å) and (0.942 Å), found at ambient conditions.[29,43] The longest hydrogen bond has an almost straight geometry with an O(w)-H(1)···O(1) bond angle of 175.9°. It is oriented almost parallel to the b axis and is responsible for the binding of the layers. The shortest hydrogen bond, O(w)-H(2)···O(2), has a bond angle of 172.1° and links the water molecules to the sulfate tetrahedra. Water molecules are not hydrogen bonded at ambient conditions but their distances decrease with pressure. In particular, the distance between $O(w_A)$ and $O(w_B)$ (Fig. 1) at 5 GPa is only 3 Å corresponding to a reduction in about 10% with respect to the ambient condition value. In Fig. 3(a) we compare the bond lengths of the two distinct hydrogen bonds as calculated from theory and as measured in experiment.[16] Both theory and experiments suggest that the hydrogen bond O(w)-H(1)···O(1) directed along b axis decreases faster with pressure than the O(w)-H(2)···O(2) bond, although the experimental data are affected by a larger scatter. We remark however that the theoretical bond lengths become almost equal and follow the same pressure behavior above about 4 GPa. In Sec. III B we will analyze the consequences that this observation has on the vibrational spectra. Calculated hydrogen-bond angles show a very weak dependence on pressure [see Fig. 3(b)]. In Fig. 4(a) we show the S-O bond distances in SO_4 versus pressure. The S-O bonds oriented toward the inner part of the layers are shorter and more compressible than the S-O bonds oriented toward the interlayer regions. Furthermore one can notice that the difference between the longest S-O and shortest S-O in the sulfate tetra-

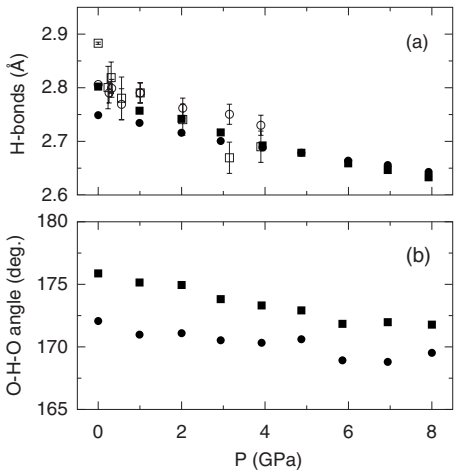

FIG. 3. (a) Hydrogen-bond lengths O(w)-H(1)···O(1) (filled squares) and O(w)-H(2)···O(2) (disks) as a function of pressure. Experimental data (open symbols) are taken from Ref. 16. (b) Hydrogen-bond angles as a function of pressure.

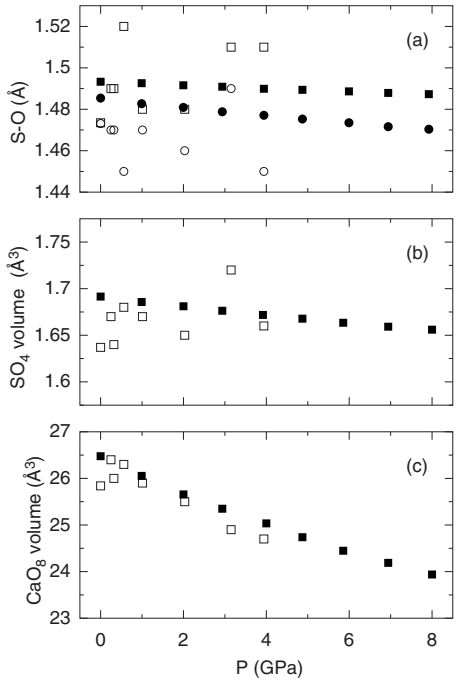

FIG. 4. (a) S-O bond distances (Å) of the shortest (circles) and longest (squares) pairs of bonds in SO_4 as a function of pressure as calculated in this work (filled symbols) and as derived from experiment (Ref. 16, open symbols). (b) Volume of the SO_4 sulfate tetrahedron and (c) of the CaO_8 polyhedra, as a function of pressure, as calculated in this work (filled squares) and as derived from experiments (Ref. 16, open squares).

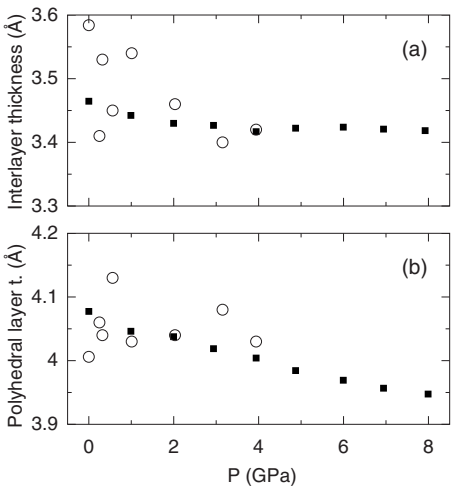

FIG. 5. (a) Interlayer and (b) polyhedral layer thicknesses as calculated in this work (filled squares) and as derived from experiment (Ref. 16, open symbols).

hedra increases with pressure, indicating that SO_4 tetrahedra are increasingly distorted for increasing pressure. Experimental data[16] show a larger distortion of the tetrahedra, however the scatter of the data and the absence of a clear trend in the experimental data suggest that these may be affected by substantial error bars. The volume of the SO_4 tetrahedra decreases slowly with pressure [Fig. 4(b)], consistently with the trend found for the average S-O bond length. In contrast, the calcium polyhedra show a much higher compressibility [Fig. 4(c)], in agreement with experiments.[16] Correspondingly, the average Ca-O bond becomes shorter, varying from 2.47 Å at ambient condition to 2.43 Å at 5 GPa. The spread of the Ca-O bonds is essentially unaffected by pressure.

In Fig. 5 we show the interlayer (water) and polyhedral (sulfate) layer thicknesses as reported in Ref. 16 and as calculated in this work. The thicknesses are calculated as distances between the planes π_1 and π_2 defined by the oxygen O(1) and O(2) in Fig. 1. Experimental points are affected by a large uncertainty and cannot be used to analyze trends. In contrast, the calculated thicknesses show much clearer pressure trends. The calculated polyhedral layer thickness shows a linear decrease, while the calculated interlayer thickness decreases at low pressure, but levels off above 2 GPa. The drastic pressure-induced reduction in the compressibility of the water layer suggests that compression of the water layer is approaching a mechanical limit and that further compression can only be achieved by means of a reorganization of the molecules in the layer. Such mechanism may be responsible for the transformation of gypsum into high-pressure phases, as discussed in Sec. IV A.

B. Infrared and Raman spectra

IR and Raman spectra are related to the dielectric response of the material to an external field, hence we begin this section by analyzing the high-frequency dielectric tensor ϵ^{∞}. The calculated high-frequency dielectric tensor of gypsum at 0 GPa is

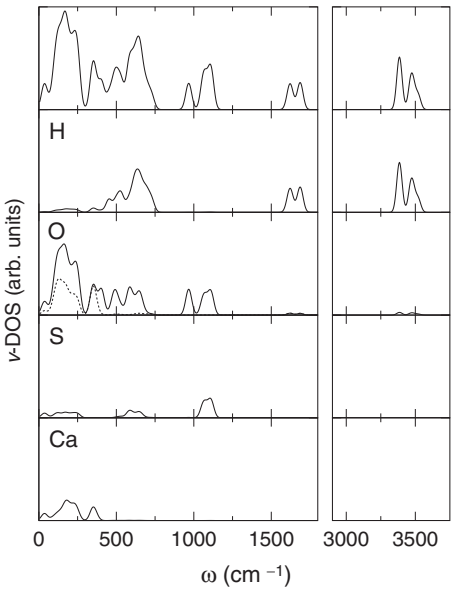

FIG. 6. Zone-center vibrational density of states of gypsum at 0 GPa and decompositions in terms of projections on H, O, S, Ca atoms. The contribution of the water molecules to the total oxygen density of states is also shown (dotted). A Gaussian broadening of 19 cm^{-1} was applied.

$$\epsilon^{\infty} = \begin{pmatrix} 2.35 & -0.02 & 0.00 \\ -0.02 & 2.37 & 0.00 \\ 0.00 & 0.00 & 2.37 \end{pmatrix}, \quad (2)$$

where the x axis is taken along a, the z axis is taken along b, and the y axis is given by the cross product of the previous directions. Even though the structure is layered (with layers oriented perpendicular to the z axis in our notation), the high-frequency dielectric tensor turns out to be fairly isotropic, with ϵ^{∞}_{yy} and ϵ^{∞}_{xx} in excellent agreement with the values of Ref. 44 ($\epsilon^{\infty}=2.358$ and $\epsilon^{\infty}=2.329$ for directions in the a-c plane) and Ref. 45, though the latter shows a larger anisotropy: $\epsilon^{\infty}=2.223$ along b while $\epsilon^{\infty}=2.2819$ and $\epsilon^{\infty}=2.4545$ in the plane a-c. By increasing pressure, we note that the high-frequency dielectric tensor becomes increasingly anisotropic, with pressure derivatives $d\epsilon^{\infty}_{xx}/dP = d\epsilon^{\infty}_{yy}/dP = 0.026$ GPa^{-1} and $d\epsilon^{\infty}_{zz}/dP = 0.036$ GPa^{-1}.

In Fig. 6 we show the vibrational density of states of gypsum at 0 GPa, calculated using zone-center modes only. The zone-center vibrational density of states, can be helpful in discussing the origin of the vibrational modes seen in IR and Raman spectroscopy, which will be discussed in the next section.[46] For example, our decomposition into atomic projections allows us to assign vibrational modes above 1500 cm^{-1} entirely to the water molecules. The hydrogen contribution is dominant in the O-H stretching and bending regions above 1500 cm^{-1} and also around 650 cm^{-1}, in the water librational region. The oxygen contribution can be subdivided in terms of water molecules and SO_4 groups. The contribution of oxygen belonging to water molecules becomes dominant above 1500 cm^{-1}, while is totally absent in the range 900–1200 cm^{-1}, where oxygen belonging to tet-

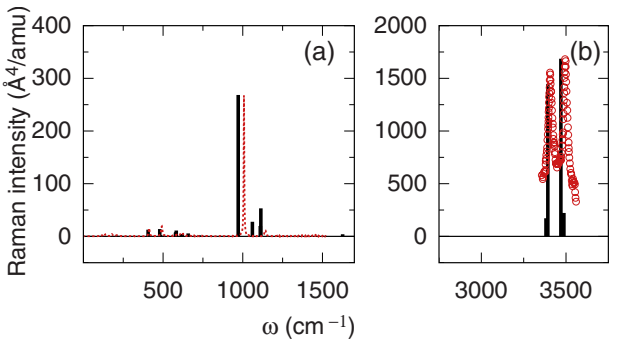

FIG. 7. (Color online) Raman spectrum of gypsum calculated at $P=0$ GPa (solid/black) compared to experimental data taken from Ref. 51. (a) Vibrational modes up to 1700 cm^{-1}. The theoretical scale is shown. Experimental data (dotted/red), originally in arbitrary units have been rescaled to match the height of the theoretical SO_4 symmetric stretching mode. (b) O-H stretching region. Experimental data (circles/red) are taken from Ref. 47.

rahedra is active. The latter constitutes the dominant part also in the SO_4 bending region (500–750 cm^{-1}) while below 400 cm^{-1} the two contributions have similar magnitude. Sulfur atoms give the largest contribution in the range 1000 cm^{-1} up to 1200 cm^{-1} corresponding to the SO_4 stretching region. The other contributions correspond to the SO_4 bending region and to the low-frequency band ($\leq$300 cm^{-1}) presumably related to SO_4 translations. The decomposition in terms of H, O, and S suggests that in the range 500–750 cm^{-1}, the gypsum vibrational modes should be considered as a mixing between water librations and SO_4 bending modes. Ca atoms contribute only below 400 cm^{-1} due to their heavier mass.

The Raman spectrum of gypsum has been the object of previous investigations,[14,15,47–50] that have clarified the origin of the majority of the features in the vibrational spectrum. However some details of the gypsum vibrational spectrum remain unclear. In particular, a debate is open on the origin of a "companion mode" of the symmetric stretching of SO_4 tetrahedra, appearing in the spectra at low temperature[50] and high pressure.[14,15] The primitive or Bravais unit cell of gypsum-I, from which selection rules are deduced[28] contains two molecular units $CaSO_4 \cdot 2H_2O$ for a total of 24 atoms. Thus, when the primitive cell is chosen, 72 normal modes are found at the center of the Brillouin zone, of which three are purely translational. Group theory analysis[28,44,50] shows that the irreducible representations correspond to,

$$\Gamma_i = 17A_g + 19B_g + 17A_u + 19A_u. \quad (3)$$

for a total of 36 Raman active modes and 33 IR active ones, consistent with the centrosymmetric character of the $C2/c$ space group. In Fig. 7 we show the calculated first-principles Raman spectrum of gypsum in the region of the SO_4 tetrahedron vibrational modes and in the region of O-H stretching modes. The spectrum is compared to the experimental results of Refs. 47 and 51. The good agreement between theory and experiment regarding the frequency position of the peaks is a further support to the validity of the approximations described in Sec. II. SO_4 stretching modes dominate the spectrum below 1700 cm^{-1}. Bending of the water molecules is located at 1630 cm^{-1} while stretching of the O-H bonds gives rise to a strong doublet located at 3393 and 3470 cm^{-1} in the theoretical spectrum. In Table II we present the calculated frequency and pressure dependence of the strongest Raman lines between 400 and 1200 cm^{-1} compared with experimental data from Refs. 15 and 50. The main Raman line in the spectrum below 1600 cm^{-1} corresponds to the symmetric stretching of the S-O bonds in the SO_4 tetrahedra,

TABLE II. Raman active SO_4 and H_2O vibrational frequencies in the range 400–1200 cm^{-1}, and their pressure derivatives. Experimental data are taken from Refs. 15 and 50 (†, temperature 77 K). ν_0 is the frequency calculated at 0 GPa.

Raman vibrational modes					
	Theory			Expt.	
ν_0	Ass.	$d\nu/dP$	ν	Ass.	$d\nu/dP$
406.1	A_g (SO_4)	3.1 (0.2)	412	A_g	0.9 (0.2)
479.2	A_g (SO_4)	4.2 (0.2)	492	A_g	3.4 (0.2)
578.1	B_g (H_2O)	1.5 (0.2)	578†	B_g†	
582.7	A_g (H_2O)	3.4 (0.3)	589†	A_g†	
616.7	B_g (SO_4)	2.2 (0.3)	621†	B_g†	
618.4	A_g (H_2O)	3.5 (0.6)	628†	A_g	1.4 (0.2)
657.5	B_g (SO_4)	4.0 (0.1)	670	B_g	0.4 (0.4)
657.0	A_g (H_2O)	5.7 (0.4)	685†	A_g	
727.4	A_g (H_2O)	5.0 (0.3)			
			990†	A_g	
971.4	A_g (SO_4)	4.5 (0.1)	1008	A_g	4.7 (0.4)
1060.3	B_g (SO_4)	2.8 (0.1)	1117†	B_g†	
1109.9	A_g (SO_4)	6.5 (0.1)	1142†	A_g†	
1113.4	B_g (SO_4)	8.2 (0.3)	1137	B_g	4.4 (0.4)

TABLE III. Infrared active SO_4 and H_2O vibrational frequencies in the range 400–1200 cm^{-1}, and their pressure derivatives. Experimental data are taken from Ref. 15 and from Ref. 52 (†). ν_0 is the frequency calculated at 0 GPa.

Infrared vibrational modes					
	Theory			Expt.	
ν_0	Ass.	$d\nu/dP$	ν	Ass.	$d\nu/dP$
451.3	B_u (H_2O)	4.6 (1.1)	463†	B_u	
527.1	B_u (H_2O)	1.4 (0.2)			
582.1	A_u (SO_4/H_2O)	4.0 (0.2)	580†	A_u	
603.3	B_u (SO_4/H_2O)	1.1 (0.2)	605		−0.6 (0.2)
643.4	B_u (SO_4/H_2O)	3.5 (0.2)	672		0.6 (0.1)
648.0	A_u (H_2O)	1.9 (0.4)			
681.8	B_u (H_2O)	3.8 (0.3)			
698.2	A_u (H_2O)	1.9 (0.4)			
962.8	A_u (SO_4)	4.3 (0.2)	1002		2.5 (0.2)
1061.1	B_u (SO_4)	3.6 (0.1)	1120	B_u†	2.6 (0.3)
1078.7	A_u (SO_4)	6.3 (0.2)	1127†	A_u	
1107.9	B_u (SO_4)	8.1 (0.2)	1150	B_u	4.6 (0.2)

occurring at 971 cm^{-1} at zero pressure. The main Raman line shifts to higher frequencies with increasing pressure. The calculated pressure derivative of this mode is in remarkably good agreement with the experimental one. The positive sign of the pressure derivative is likely to be a consequence of the shortening of the S-O bonds. Asymmetric stretching gives rise to peaks at 1060, 1110, and 1113 cm^{-1} at the right side of the main Raman line. Bending modes of the SO_4 tetrahedra, rotations and translations of the water molecules are responsible of the peaks in the range 400–600 cm^{-1}.[50] As observed by Berenblut *et al.*,[49] the half width of the sulfate bands in the range 400–620 cm^{-1} is clearly affected by the presence of water molecules forming hydrogen bonds. This is consistent with the analysis of the vibrational density of states presented in the previous section, where we show that sulfate and water modes are both active in this frequency region. In Table III we present the calculated frequency and pressure dependence of the strongest IR lines between 400 and 1200 cm^{-1} together with their pressure dependence, and compare them with experimental data from Refs. 15 and 50. We note that the pressure behavior of the infrared modes follows closely the one reported above for the Raman modes.

In Table IV we show the pressure dependence $d\nu/dP$ of the frequencies ν of the infrared and Raman modes related to water molecules, compared to the experimental data from Refs. 15 and 50. Both the frequencies and their pressure dependence compare fairly well with the experimental data. The two strong Raman modes in the O-H stretching region arise from the stretching of the O-H bonds parallel to the $CaSO_4$ layers (3393 cm^{-1}), and from the stretching of the O-H bonds along the *b* axis, and thus perpendicular to the layers (3470 cm^{-1}), in agreement with the discussion reported in Ref. 47. At zero pressure each one of the four Raman stretching modes is localized over the four O-H bonds directed along *b* (high-frequency stretching) or over the four O-H bonds parallel to the layers (low-frequency stretching). At 5 GPa the two most intense modes can still be largely characterized as parallel and perpendicular to the layers but each mode shows now an increased delocalization over the two O-H bonds of the same molecule. This is consistent with the fact that at 5 GPa the calculated hydrogen bonds become approximately equal [see Fig. 3(a)]. A similar behavior is observed for the frequency and pressure dependence of the IR stretching modes (see Table IV). Raman and IR vibrational frequencies corresponding to the water bending appear to be pressure independent or weakly affected.

IV. HIGH-PRESSURE PHASE OF GYPSUM

Available experimental evidence suggests that gypsum undergoes one or more phase transitions starting from a pressure of about 5 GPa.[14–16] Experimental data however suggest that the structural changes are not extensive and are limited to local distortions of the sulfate tetrahedra and/or to reorientation of the water molecules. With this in mind, we carried out a search for the high-pressure phases of gypsum by means of constant-pressure MD starting from gypsum-I. We adopted the conventional unit cell of gypsum-I (48 atoms) as the starting configuration. The MD run was carried out at a temperature of 500 K and at a pressure of 10 GPa. After about 10 ps of MD, the resulting structure was relaxed at various pressures between 2 and 10 GPa by means of damped dynamics. The relaxed structures were then further optimized with norm-conserving pseudopotentials. In Fig. 8 we show the HP structure of gypsum resulting from our simulations at 5 GPa.[53] In Fig. 9(a) we show the energy of gypsum-I and of the HP structure as a function of volume. The curves are fitted with a Murnaghan equation of state.[54] The fit yields a bulk modulus of 49.2 GPa with a pressure derivative of 3.5 for the high-pressure structure while for phase I it gives 56.7 GPa and 2.2 for its pressure derivative. The bulk modulus for phase I is larger than the experimental

TABLE IV. Frequencies and their pressure dependence $d\nu/dP$ for the infrared and Raman-active vibrational modes of the water molecules in gypsum. Experimental data are taken from Refs. 15 and 50 (indicated by *). Frequencies ν and pressure derivatives $d\nu/dP$ are given in cm^{-1} and cm^{-1}/GPa, respectively.

Raman vibrational modes					
	Theory			Expt.	
ν (0 GPa)	Ass.	$d\nu/dP$	ν	Ass.	$d\nu/dP$
3487.4	B_g	−7.3 (0.9)	3490	B_g	-14.4 ± 0.2
3469.7	A_g	−6.1 (1.1)	3479	A_g	-6.9 ± 0.5
3392.7	A_g	−3.2 (0.5)	3405	A_g+B_g	1.0 ± 1.0
3381.6	B_g	−2.9 (0.4)	3402*		
1686.0 (weak)	B_g	0.4 (0.1)	1679*		
1626.7	A_g	−1.7 (0.7)	1629*		
Infrared vibrational modes					
	Theory			Expt.	
ν (0 GPa)	Ass.	$d\nu/dP$	ν	Ass.	$d\nu/dP$
3521.5	A_u	−5.4 (0.8)	3546	A_u	-4.8 ± 0.3
3466.5	B_u	−8.4 (1.1)	3482	B_u	-9.3 ± 0.9
3383.8	B_u	−2.6 (0.5)	3406	B_u	2.2 ± 0.9
3382.1 (weak)	A_u	−1.9 (0.4)			
1686.5	A_u	0.10 (0.03)	1690	A_u	0.2 ± 0.1
1615.8	B_u	−1.8 (0.1)	1627	B_u	-1.4 ± 0.1

estimate of about 45 GPa.[16,32] The discrepancy may originate from our choice of the exchange and correlation functional, as well as from the fact that our calculations are performed at zero temperature. However the calculated pressure derivative of the bulk modulus is smaller than the experimental one (3.3, Ref. 16). Consequently the discrepancy between experiment and theory for the volume of gypsum-I at about 4 GPa is still as small as 1%.

From the energy-volume equation of state we derived the enthalpies of the two structures [Fig. 9(b)]. The enthalpy of the HP structure becomes lower than gypsum-I at a pressure of about 4.7 GPa, indicating that above this pressure the HP structure is more stable than gypsum-I. Although we cannot rule out the existence of other structures with lower enthalpies, should such structures exist, they would have to become more stable than gypsum-I at a lower pressure than the HP structure proposed here. This is difficult to reconcile with the experimental evidence that gypsum-I is stable up to about 4 GPa. With the caveat that the enthalpy difference between gypsum-I and the HP structure is rather small, and so the possibility exists that other structures with similar molecular

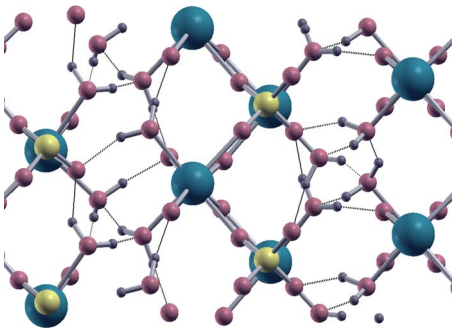

FIG. 8. (Color online) Ball and stick model of the high-pressure structure of gypsum at 5 GPa. Ca atoms (green), S atoms (yellow), O atoms (pink), H atoms (gray), and hydrogen bonds (dotted lines) are shown. The size of the balls is in the order: Ca (largest), S, O, and H.

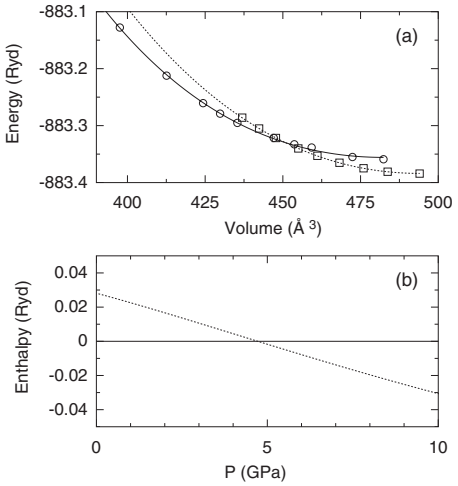

FIG. 9. (a) Energy as a function of volume for the high-pressure model structure (circles) and for gypsum-I (empty squares). Data are fitted with a Murnaghan equation of state (solid and dotted lines). (b) Enthalpy as a function of pressure for gypsum-I (solid) and for the high-pressure model structure (dotted).

arrangements could have comparable enthalpies, we can conclude that our results support the notion that a phase transition takes place in gypsum in the vicinity of 5 GPa, as reported by several experimental groups.[15,16] In particular, the transition appears to be a consequence of the rearrangement of the hydrogen bonds leading to the collapse of the interlayer distance, as described in detail in the next section.

A. Structure

The most remarkable differences between gypsum-I and our HP structure are (i) the collapse of the interlayer distance in HP gypsum, (ii) the reorientation of the water molecules, and (iii) the sliding of the sulfate layers. The collapse of the interlayer distance and the reorientation of the water molecules are connected with a substantial rearrangement of the hydrogen-bond network. Although the total number of hydrogen bonds is the same in the low- and high-pressure structures, water molecules form hydrogen bonds with neighboring water molecules in the HP structure. No water-water hydrogen bonds were present in gypsum-I. The new bonds replace hydrogen bonds originally binding water molecules to oxygen belonging to the sulfate layers. Hydrogen-bond lengths are comparable in the low- and high-pressure structures, with an average hydrogen-bond length of 2.68 Å in the HP structure, which compares well with the value obtained for phase I at 5 GPa (Fig. 3). The spread of the hydrogen-bond distribution, about 0.05 Å is slightly larger than the difference between the two types of bond reported in Fig. 3. Moreover, the large scatter in the distribution of bond lengths is suggestive of a possible disordering of the water sublattice in the HP phase. The average hydrogen-bond O-H···O angle is 157.6° (with a standard deviation of 8.6°), substantially lower than in gypsum-I at the same pressure of 5 GPa (~172°). We also notice the occurrence of very short hydrogen bonds (~2.55 Å) in the HP structure. The reorientation of the water molecules and the consequent changes in the hydrogen-bond network are consistent with the observed collapse of the interlayer distance in the HP structure. The average interlayer thickness in the HP structure at 5 GPa is 3.06 Å corresponding to an average reduction of 0.36 Å with respect to gypsum I at the same pressure. On the other hand the polyhedral layer thickness is 4.05 Å in the HP structure, slightly larger than in gypsum-I (Fig. 5). It is interesting to remark that the collapse takes place along the *b* axis of gypsum-I, i.e., the axis with the largest nonlinear decrease in the compressibility. We argue that the nonlinear behavior observed and calculated for the compressibility along *b* signals a mechanical limit to the decrease in the interlayer distance in gypsum-I. Further compression beyond this limit requires a reorganization of the water molecules, which is eventually achieved through a phase transition into the HP structure.

The degree of distortion of the SO_4 tetrahedra in the HP structure is similar to the one calculated in gypsum-I. The average S-O bond in HP gypsum is 1.484 Å with a standard deviation of 0.010 Å while the average Ca-O bond is 2.409 Å with a standard deviation of 0.059 Å. Distortion of the polyehdra does not appear to be qualitatively different in the two structures. In Fig. 10 we show the volume versus pressure behavior of gypsum-I and of the HP structure, and we compare our results with experimental data from Refs. 16 and 32. Our results for gypsum-I are in close agreement with the data of Ref. 16. Moreover, the calculated volume of the HP structure is consistent with the jump in volume measured experimentally.

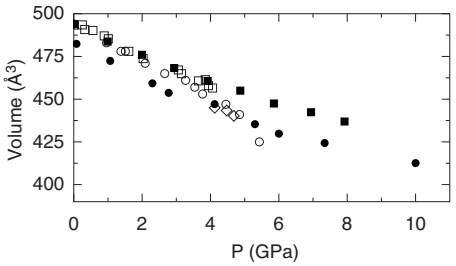

FIG. 10. Volume of the unit cell of the HP structure (filled circles) and of phase I (filled squares), as a function of pressure. Experimental data are from Ref. 16 (empty squares refer to gypsum-I, diamonds to the HP structure) and Ref. 32 (empty circles).

B. Infrared and Raman vibrational spectra

In Fig. 11 we compare the zone-center vibrational density of states of the HP gypsum model to that of gypsum-I. For consistency, the two spectra are calculated considering the $q=0$ modes of a periodic cell containing 48 atoms, which in the case of gypsum-I corresponds to the conventional monoclinic unit cell used as the initial cell for the MD search. The comparison shows that the vibrational bands below 600 cm^{-1} are almost unaffected by the transition, which is consistent with the small structural changes undergone by the CaO_8 and SO_4 polyhedra across the transition. The larger differences can be identified in regions of the spectrum dominated by the water vibrations, i.e., around 650, 1600, and 3000–3500 cm^{-1}. The water librational region (around 650 cm^{-1}) is broader in the HP structure than in gypsum-I. Moreover the gap between the water librational region and the SO_4 stretching modes (750–900 cm^{-1}) is completely filled in the vibrational density of states of the HP structure. This is consistent with the increase in IR intensity observed in the same frequency range by Knittle *et al.* (Ref. 15) upon increasing pressure from 3 to 6 GPa. Their spectrum at 6

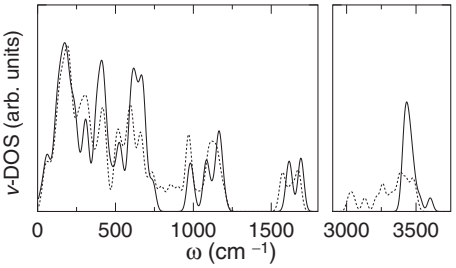

FIG. 11. Zone-center vibrational density of states of the HP structure (dotted) and phase I (solid) of gypsum at 5 GPa. A Gaussian broadening of 19 cm^{-1} was applied.

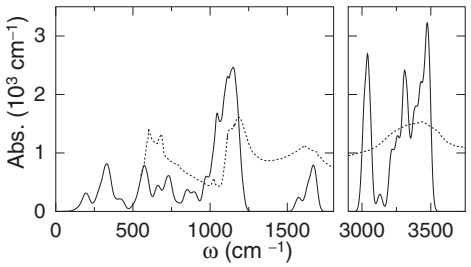

FIG. 12. Theoretical infrared absorption spectrum of the HP gypsum structure at 5 GPa. A Gaussian broadening of 19 cm^{-1} was applied (Ref. 55). The experimental spectrum (arb. units, Ref. 15) at 6 GPa is also reported for comparison.

GPa is compared with our calculated IR data in Fig. 12.

We now turn to the Raman spectrum and focus on the sharp mode located slightly below 1000 cm^{-1} [see Fig. 13(a)]. The mode corresponds to the symmetric stretching of the S-O bonds and is the analog of the sharp mode present in the spectrum of gypsum-I at about the same frequency [see Fig. 7]. As mentioned in Sec. III B, the mode was reported to undergo an apparent splitting at pressures above ~4 GPa, with a companion mode appearing about 20 cm^{-1} below the original mode. The new mode was observed to increase gradually in amplitude relative to the original mode, the latter disappearing above 6 GPa.[15,49] Our finding that the sharp peak in the Raman spectra shifts from 994 cm^{-1} in gypsum-I to 970 cm^{-1} in the HP structure at the same pressure (5 GPa) is consistent with the interpretation of the experimental splitting as arising from the transformation of gypsum-I into a HP phase, as suggested in Refs. 14 and 15.

A second remarkable difference between the calculated spectra of gypsum-I and of the HP structure can be identified in the O-H stretching region. The width of the Raman and IR bands doubles in the HP structure, relative to gypsum-I [see Figs. 12 and 13(b)]. A similar broadening is also observed in the experimental infrared and Raman spectra at high pressure.[14,15] We trace the large width of the water stretching region to the overall strengthening of the hydrogen bonds and to the formation of new types of hydrogen bonds (water-water) in the HP structure.

V. CONCLUSIONS

Our results for the structural parameters and vibrational spectra of gypsum-I are in excellent agreement with experimental data up to the limit of its stability range, around 4 GPa. Pressure-induced changes in the vibrational spectra are attributed mainly to distortions of the water molecules. At about 5 GPa we find that a structure with collapsed interlayer distance and substantial rearrangement of the hydrogen bonds becomes energetically more stable than gypsum-I. The calculated vibrational spectra of this structure show remarkable agreement with the spectra reported by various authors for the high-pressure phases of gypsum. We conclude that our high-pressure structure is an excellent model for the high-pressure phases of gypsum reported by Knittle *et al.* (Ref. 15) and by Huang *et al.* (Ref. 14). We suggest that future analyses of the x-ray diffraction data taken beyond the stability range of gypsum-I include models with similar structural features in the refinement of the data. Our finding that compression in gypsum takes place predominantly by means of a rearrangement of the water layer offers a structural model for the retention of water in molecular form which may have implications for our understanding of dehydration and water storage of minerals in the upper mantle.

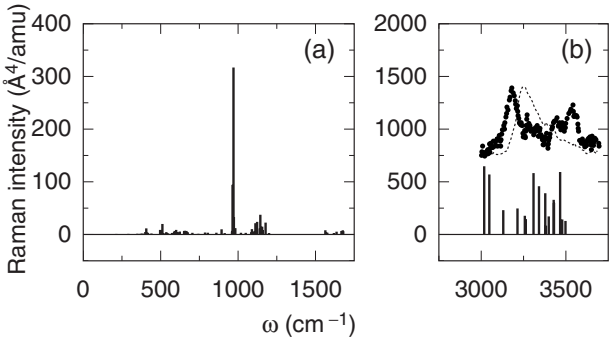

FIG. 13. (a) Theoretical Raman spectrum of the high-pressure gypsum structure at 5 GPa. (b) Comparison in the O-H stretching region with experimental spectra at 5.5 (dotted) and 8 GPa (disks) from Ref. 14.

ACKNOWLEDGMENTS

We acknowledge useful discussions with Paola Comodi and Sabrina Nazzareni. We also acknowledge support from Consiglio Nazionale delle Ricerche (CNR) through the project "EuroSlab" of the EuroMinScI/ESF iniziative.

[1] B. H. Horgan, J. F. Bell III, E. Z. Noe Dobrea, E. A. Cloutis, D. T. Bailey, M. A. Craig, L. H. Roach, and J. F. Mustard, J. Geophys. Res. **114**, E01005 (2009).

[2] M. Murakami, K. Hirose, H. Yurimoto, S. Nakashima, and N. Takafuji, Science **295**, 1885 (2002).

[3] S. Ono, J. Geophys. Res. **103**, 18253 (1998).

[4] M. Faccenda, L. Burlini, T. V. Gerya, and D. Mainprice, Nature (London) **455**, 1097 (2008); L. Burlini and D. Bruhn, Geol. Soc. London, Spec. Publ. **245**, 1 (2005).

[5] E. Huang, A. Li, J. A. Xu, R. J. Chen, and T. Yamanaka, Geophys. Res. Lett. **23**, 3083 (1996).

[6] H. Liu, J. Hu, J. Xu, Z. Liu, J. Shu, H. K. Mao, and J. Chen, Phys. Chem. Miner. **31**, 240 (2004).

[7] C. T. Johnston, S. L. Wang, D. L. Bish, P. Dera, S. F. Agnew, and J. W. Kenney, Geophys. Res. Lett. **29**, 1770 (2002); P. Dera, C. T. Prewitt, S. Japel, D. L. Bish, and C. T. Johnston, Am. Mineral. **88**, 1428 (2003).

[8] T. Nagai, T. Ito, T. Hattori, and T. Yamanaka, Phys. Chem.

Miner. **27**, 462 (2000).
[9] J. H. Nguyen, M. B. Kruger, and R. Jeanloz, Phys. Rev. Lett. **78**, 1936 (1997).
[10] S. R. Shieh and T. S. Duffy, Phys. Rev. B **66**, 134301 (2002).
[11] M. B. Kruger, Q. Williams, and R. Jeanloz, J. Chem. Phys. **91**, 5910 (1989).
[12] S. Raugei, P. L. Silvestrelli, and M. Parrinello, Phys. Rev. Lett. **83**, 2222 (1999).
[13] M. Mookherjee and L. Stixrude, Am. Mineral. **91**, 127 (2006).
[14] E. Huang, J.-A. Xu, J.-F. Lin, and J.-Z. Hu, High Press. Res. **17**, 57 (2000).
[15] E. Knittle, W. Phillips, and Q. Williams, Phys. Chem. Miner. **28**, 630 (2001).
[16] P. Comodi, S. Nazzareni, P. F. Zanazzi, and S. Speziale, Am. Mineral. **93**, 1530 (2008).
[17] I. Daniel, G. Fiquet, P. Gillet, M. W. Schmidt, and M. Hanfland, Eur. J. Mineral. **12**, 721 (2000); T. B. Ballaran and R. J. Angel, *ibid.* **15**, 241 (2003).
[18] E. Libowitzky and G. R. Rossman, Am. Mineral. **82**, 1111 (1997).
[19] B. Winkler, Phys. Chem. Miner. **23**, 310-318 (1996).
[20] A. M. Hofmeister, H. Cynn, P. C. Burnley, and C. Meade, Am. Mineral. **84**, 454 (1999).
[21] M. W. Schmidt, Am. Mineral. **80**, 1286 (1995); G. L. Clarke, R. Powell, and J. A. Fitzherbert, J. Metamorph. Geol. **24**, 715 (2006); B. A. Kolesov, G. A. Lager, and A. J. Schultz, Eur. J. Mineral. **20**, 63 (2008).
[22] P. Comodi, P. Fumagalli, S. Nazzareni, and P. F. Zanazzi, Am. Mineral. **90**, 1012 (2005); P. Fumagalli and L. Stixrude, Earth Planet. Sci. Lett. **260**, 212 (2007).
[23] N. J. Chinnery, A. R. Pawley, and S. M. Clark, Science **286**, 940 (1999).
[24] P. W. Mirwald, J. Chem. Phys. **128**, 074502 (2008).
[25] E. S. Robinson, *Basic Physical Geology* (Wiley, New York, 1982).
[26] J. M. Garcia-Ruiz, R. Villasuso, C. Ayora, A. Canals, and F. Otalora, Geology **35**, 327 (2007).
[27] M. Atoji and R. E. Rundle, J. Chem. Phys. **29**, 1306 (1958).
[28] M. Hass and G. B. B. M. Sutherland, Proc. R. Soc. London, Ser. A **236**, 427 (1956).
[29] B. F. Pedersen and D. Semmingsen, Acta Crystallogr., Sect. B: Struct. Crystallogr. Cryst. Chem. **38**, 1074 (1982).
[30] S. Follner, A. Wolter, K. Helming, C. Silber, H. Bartels, and H. Follner, Cryst. Res. Technol. **37**, 207 (2002).
[31] A. Fernández-Martínez, G. J. Cuello, M. R. Johnson, F. Bardelli, G. Román-Ross, L. Charlet, and X. Turrillas, J. Phys. Chem. A **112**, 5159 (2008).
[32] I. C. Stretton, P. F. Schofield, S. Hull, and K. S. Knight, Geophys. Res. Lett. **24**, 1267 (1997).
[33] A. R. Oganov, J. P. Brodholt, and G. D. Price, *Energy Modelling in Minerals*, edited by C. M. Gramaccioli, EMU Notes in Mineralogy Vol. 4 (Eötvös University Press, Budapest, 2002), Chap. 5, p. 83.
[34] M. J. Gillan, D. Alfè, J. Brodholt, L. Vočadlo, and G. D. Price, Rep. Prog. Phys. **69**, 2365 (2006).
[35] S. Scandolo, P. Giannozzi, C. Cavazzoni, S. de Gironcoli, A. Pasquarello, and S. Baroni, Z. Kristallogr. **220**, 574 (2005).
[36] P. Giannozzi, S. Baroni, N. Bonini, M. Calandra, R. Car, C. Cavazzoni, D. Ceresoli, G. L. Chiarotti, M. Cococcioni, I. Dabo, A. Dal Corso, S. de Gironcoli, S. Fabris, G. Fratesi, R. Gebauer, U. Gerstmann, C. Gougoussis, A. Kokalj, M. Lazzeri, L. Martin-Samos, N. Marzari, F. Mauri, R. Mazzarello, S. Paolini, A. Pasquarello, L. Paulatto, C. Sbraccia, S. Scandolo, G. Sclauzero, A. P. Seitsonen, A. Smogunov, P. Umari, and R. M. Wentzcovitch, J. Phys.: Condens. Matter **21**, 395502 (2009).
[37] J. P. Perdew, K. Burke, and M. Ernzerhof, Phys. Rev. Lett. **77**, 3865 (1996).
[38] S. Baroni, S. de Gironcoli, A. Dal Corso, and P. Giannozzi, Rev. Mod. Phys. **73**, 515 (2001).
[39] M. Lazzeri and F. Mauri, Phys. Rev. Lett. **90**, 036401 (2003).
[40] R. Car and M. Parrinello, Phys. Rev. Lett. **55**, 2471 (1985).
[41] M. Parrinello and A. Rahman, J. Appl. Phys. **52**, 7182 (1981).
[42] D. Vanderbilt, Phys. Rev. B **41**, 7892 (1990).
[43] V. Seidl, O. Knop, and M. Falk, Can. J. Chem. **47**, 1361 (1969).
[44] K. Iishi, Phys. Chem. Miner. **4**, 341 (1979).
[45] J. R. Aronson, A. G. Emslie, E. V. Miseo, E. M. Smith, and P. F. Strong, Appl. Opt. **22**, 4093 (1983).
[46] L. Giacomazzi, P. Umari, and A. Pasquarello Phys. Rev. B **79**, 064202 (2009).
[47] R. Couty, B. Velde, and J. M. Besson, Phys. Chem. Miner. **10**, 89 (1983).
[48] R. G. Dickinson and R. T. Dillon, Proc. Natl. Acad. Sci. U.S.A. **15**, 695 (1929).
[49] B. J. Berenblut, P. Dawson, and G. R. Wilkinson Spectrochim. Acta, Part A **27**, 1849 (1971); **29**, 29 (1973).
[50] N. Krishnamurty and V. Soots, Can. J. Phys. **49**, 885 (1971).
[51] http://rruff.info/gypsum/display=default/R040029 (source: University of Arizona Mineral Museum 4885).
[52] G. Schaack, Phys. Kondens. Mater. **1**, 245 (1963).
[53] See supplementary material at http://link.aps.org/supplemental/10.1103/PhysRevB.81.064103 for the structural parameters of the HP model structure (cell parameters and atomic positions).
[54] F. D. Murnaghan, Proc. Natl. Acad. Sci. U.S.A. **30**, 244 (1944).
[55] We calculated the absorption spectrum from the knowledge of the dielectric function by exploiting the same postprocessing tools adopted in Ref. 56.
[56] L. Giacomazzi and P. Umari, Phys. Rev. B **80**, 144201 (2009).